

# Atom chip apparatus for experiments with ultracold rubidium and potassium gases

M. K. Ivory,<sup>1</sup> A. R. Ziltz,<sup>1</sup> C. T. Fancher,<sup>1</sup> A. J. Pyle,<sup>1</sup> A. Sensharma,<sup>1</sup> B. Chase,<sup>1</sup> J. P. Field,<sup>1</sup> A. Garcia,<sup>1</sup> D. Jervis,<sup>2</sup> and S. Aubin<sup>1,a)</sup>

<sup>1</sup>*Department of Physics, College of William and Mary, Williamsburg, Virginia 23187, USA*

<sup>2</sup>*Department of Physics, University of Toronto, Toronto, Ontario M5S 1A7, Canada*

(Received 29 October 2013; accepted 16 March 2014; published online 4 April 2014)

We present a dual chamber atom chip apparatus for generating ultracold  $^{87}\text{Rb}$  and  $^{39}\text{K}$  atomic gases. The apparatus produces quasi-pure Bose-Einstein condensates of  $10^4$   $^{87}\text{Rb}$  atoms in an atom chip trap that features a dimple and good optical access. We have also demonstrated production of ultracold  $^{39}\text{K}$  and subsequent loading into the chip trap. We describe the details of the dual chamber vacuum system, the cooling lasers, the magnetic trap, the multicoil magnetic transport system, the atom chip, and two optical dipole traps. Due in part to the use of light-induced atom desorption, the laser cooling chamber features a sufficiently good vacuum to also support optical dipole trap-based experiments. The apparatus is well suited for studies of atom-surface forces, quantum pumping and transport experiments, atom interferometry, novel chip-based traps, and studies of one-dimensional many-body systems. © 2014 AIP Publishing LLC. [<http://dx.doi.org/10.1063/1.4869781>]

## I. INTRODUCTION

The discovery of ultracold quantum degenerate atomic gases has opened up a wide range of physical phenomena for exploration with the high precision techniques of atomic physics. The exquisite experimental controls, high resolution probes, tunability of atomic interactions via Feshbach resonances, and long coherence times of these ultracold atomic systems has enabled their use in experimental investigations of complex many-body systems.<sup>1</sup> Furthermore, the coherence of these gases has advanced the development of matter-wave interferometry with an eye towards precision measurements of forces.<sup>2,3</sup> Finally, the availability of both bosonic and fermionic atoms can be used to study and extend the role of quantum statistics in these phenomena.

The development of atom chip micro-magnetic traps based on micro-fabricated wires on insulating substrates has further expanded the experimental control of ultracold gases.<sup>4</sup> These chips allow for the compact and efficient integration of tailored magnetic, electric, radio-frequency (RF), and optical fields for manipulating quantum gases that are otherwise not practical. In particular, this ability to sculpt both DC and RF near fields has enabled the development of compact atom interferometers,<sup>5</sup> atomic clocks,<sup>6</sup> and quantum gates.<sup>7</sup> The presence of a nearby surface has also made atom chips a convenient testing ground of the Casimir-Polder force between an atom and a surface.<sup>8</sup>

In this paper, we present an atom chip-based apparatus that is well suited for studies of atom-surface forces, interferometry, transport in quasi-one-dimensional (1D) quantum gases,<sup>9</sup> and the development of novel chip-based traps. The apparatus has two vacuum chambers: atoms are collected in a vapor-loaded magneto-optical trap (MOT) situated in a first glass cell and are then loaded into a magnetic trap and transported to an atom chip in a second chamber which features an

isolated vacuum, precision magnetic field control, and superior optical access. The two chambers are connected by a set of narrow vacuum connections around a corner, so that any atoms dispensed into the MOT cell cannot travel directly to the atom chip surface. The apparatus is designed to be capable of producing ultracold quantum gases of bosonic  $^{87}\text{Rb}$ ,  $^{39}\text{K}$ , and  $^{41}\text{K}$  and fermionic  $^{40}\text{K}$ . The potassium isotopes are particularly useful for our planned experiments due to their relatively small ground level hyperfine splittings and abundant low magnetic field Feshbach resonances<sup>10-13</sup> for wide tuning of inter-atom interactions. At present, we have successfully produced Bose-Einstein condensates (BEC) of  $^{87}\text{Rb}$  with the atom chip and loaded  $^{39}\text{K}$  atoms into the chip trap. Notably, the vacuum in the MOT cell is sufficiently good that we have implemented a crossed-dipole trap loaded from a quadrupole magnetic trap,<sup>14</sup> which can also accommodate experiments.

The paper is structured in the following manner. In Sec. II, we describe the various components of the apparatus. In Sec. III, we present the performance of the apparatus as a whole, from the collection of laser cooled atoms to quantum degeneracy on the atom chip. In Sec. IV, we conclude by discussing the prospects for the apparatus and future planned experiments.

## II. APPARATUS

The design of the apparatus is determined by the types of atom chip-based experiments that it will support. In particular, precision atom-surface force measurements of the Casimir-Polder force require a stable and constant surface, which thus cannot be subject to the alkali vapor pressures of a MOT.<sup>15</sup> This requirement imposes a two chamber design with a MOT cell for laser cooling and a science cell for the atom chip. Even with this design, care must be taken to maintain a clean surface, since atoms transported into the science cell can be an inadvertent source of contamination,<sup>16,17</sup> albeit smaller. A two chamber apparatus requires a cold atom transport

<sup>a)</sup>Electronic mail: [saubi@wm.edu](mailto:saubi@wm.edu)

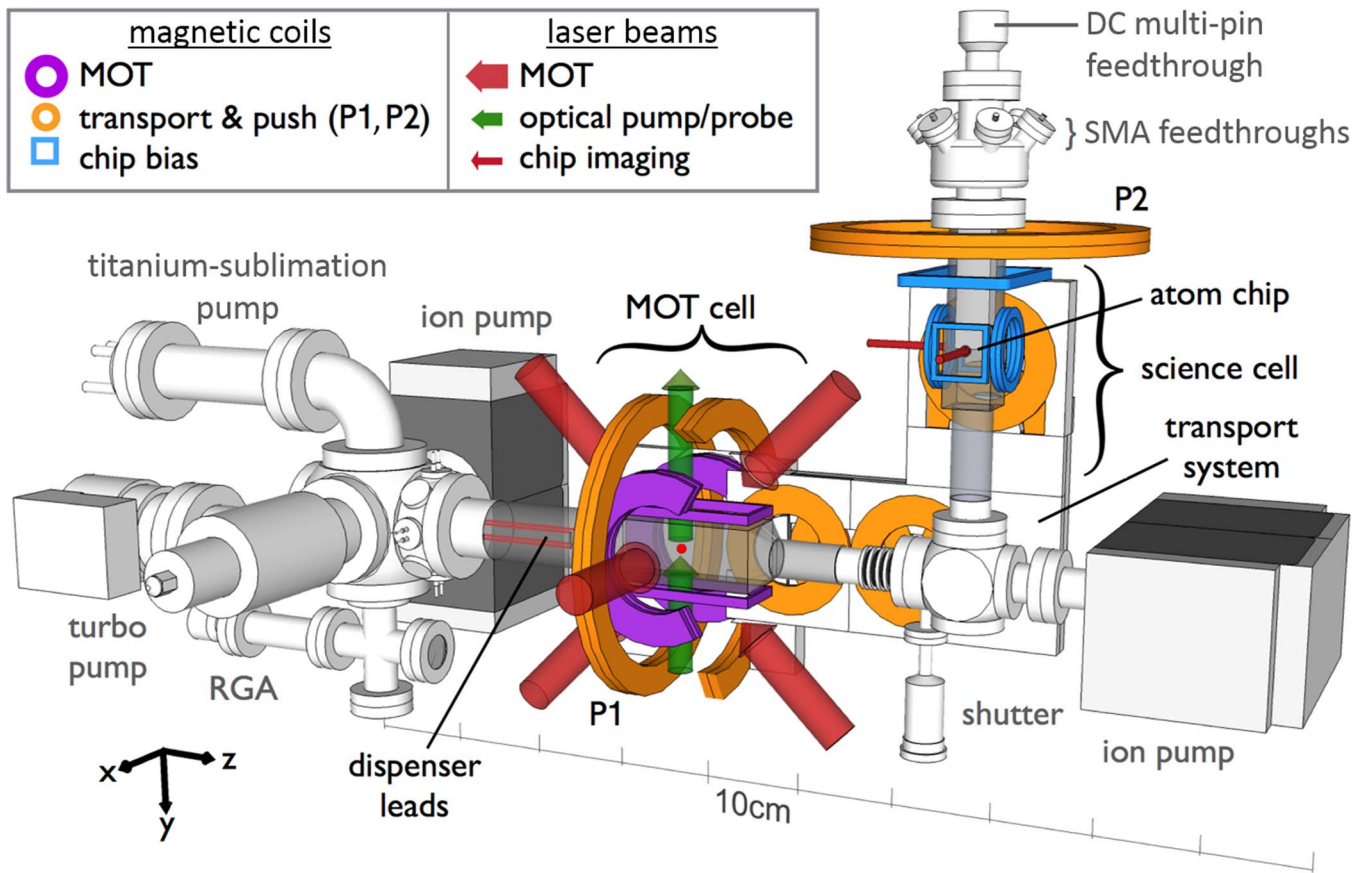


FIG. 1. Ultracold atom vacuum apparatus. The figure shows the vacuum system components (gray labels), laser beams, dual-species MOT and transport magnetic coils, and atom chip. (Large red arrows) dual-species MOT trapping beams. (Green arrows) Optical pumping and MOT absorption imaging beams. (Small red arrows) Atom chip absorption imaging beams. (Purple coils) MOT anti-Helmholtz coils (a portion of the foreground coil has been removed to show the MOT region) and MOT bias coils. Orange coils: Transport system coils; P1: MOT cell push coil pair; and MOT bias coils; P2: atom chip push coil. The foreground half of the transport system and part of coil P1 have been omitted to show the vacuum system. (Blue coils) Atom chip biasing coils. The coordinate system is consistent with that of Figure 8.

system and generally has a longer quantum gas production cycle. However, the science cell benefits from improved optical access, while also opening up space for experiments in the MOT cell.

We have chosen to use an atom chip for its proven ability to support atom interferometry experiments<sup>5</sup> and produce quasi-1D traps, as well as its potential for generating complex RF magnetic near-fields.<sup>7</sup> Furthermore, atom chips benefit from tight confinement and rapid thermalization times, which are essential for efficient evaporative cooling and sympathetic cooling. Conveniently, a change in experiment generally requires only a change in atom chip and minor modifications to the rest of the apparatus.

Figure 1 shows an overall schematic of the vacuum apparatus. The experimental system is a complex combination of vacuum, optical, and electronic components, which are carefully integrated in space. Moreover, accurate temporal integration of these components is also essential. The proper temporal sequencing of all the different components is quite intricate and requires the use of a dedicated sequencer (AdWin-Pro II) for controlling 26 analog signals and 29 digital signals that must be varied with  $\mu\text{s}$ -level accuracy over the course of the 40 s BEC production cycle. In Subsections II A–II G, we present the details of the vacuum system, laser

cooling system, magnetic trap, transport system, atom chip, imaging systems, and optical dipole traps.

## A. Vacuum system

The vacuum system design is driven by the necessity of keeping the chip surface as clean as possible and free of possible contaminants from the vapor-loaded MOT. As shown in Figure 1, the MOT and chip are in two separate, double-ended, rectangular glass cells (Technical Glass) connected via a vacuum constriction with a corner to eliminate line-of-sight atomic trajectories between the two cells. A vacuum shutter placed along this path can be used to further isolate the two cells. The atom chip science cell is vertically oriented to ensure long time-of-flight (TOF) imaging for atoms released from the chip trap.

### 1. MOT cell

The MOT cell is a rectangular Pyrex cell with external dimensions 17 cm in length and 6.3 cm in width and height. Both sides of the cell are connected to cylindrical glass necks which then transition via glass-to-metal seals to steel Conflat flanges with diameters 2.75 in. and 4.5 in. A formed

bellows connects the glass-to-metal seal to the 2.75 in. flange and allows the 51 cm length of the entire cell fitting to be adjusted by a few millimeters. This bellows also relieves mechanical stresses in the cell components and interfaces during bake-outs.

The MOT cell is connected to a 4.5 in. Conflat six-way vacuum cube that supports a 55 l/s ion pump, a titanium-sublimation pump (TSP), an all-metal angle valve, a residual-gas analyzer (RGA), and a vacuum viewport. The ion pump (Varian StarIon Plus 55) operates at 7 kV and is the primary pump for the MOT cell. The TSP assembly (Gamma Vacuum) is attached to the six-way cube via a 4.5 in. Conflat right-angle elbow. The TSP provides a calculated pumping speed of about 60 l/s, but in practice it is used as a back-up pump and is rarely activated (about once per year). The all-metal angle valve provides a connection for a 60 l/s turbo-molecular pump (Pfeiffer) used for initial pump down and bake-out. The RGA (ExTorr XT100) is installed on a four-way cross with a vacuum viewport for independent verification of filament operation. The RGA ion gauge indicates that the vacuum is in the low  $10^{-10}$  Torr range, due almost exclusively to hydrogen.

## 2. Atom chip cell

The atom chip science cell and the MOT cell are both connected, at right angles, to a custom four-port 2.75 in. cube (Kimball Physics). A custom vacuum shutter (Huntington Mechanical Laboratories) is sandwiched between this cube and the flange of the MOT cell and provides the ability to isolate the vacuums of the MOT cell and the science cell from each other. A 40 l/s ion pump at 7 kV (Varian VacIon Plus 40), powered by the same controller as the other ion pump, maintains the vacuum of the atom chip cell. This ion pump has a line-of-sight view of the MOT and its dispensers for additional pumping of the MOT cell. A viewport on the bottom of the cube provides a direct but distant view of the atom chip.

The science cell is a smaller version of the MOT cell. It features a double-ended rectangular cell (7.7 cm  $\times$  4.6 cm  $\times$  4.6 cm) with steel flanges. One of these flanges is a 2.75 in. Conflat that connects to the four-port cube, while the other end of the cell has a 3.375 in. Conflat flange that connects to a custom multiport flange (McCallister Technical Services). This multiport flange provides all the electrical connections for the atom chip via a central 2.75 in. port with a 20-pin DC electrical feedthrough and six 1.33" ports with SMA RF feedthroughs.

## 3. Atom sources

Two rubidium and two potassium dispensers (SAES and Alvac) supply the MOT cell with  $^{85}\text{Rb}$ ,  $^{87}\text{Rb}$ ,  $^{39}\text{K}$ ,  $^{40}\text{K}$ , and  $^{41}\text{K}$ . All of these isotopes are bosonic with the exception of fermionic  $^{40}\text{K}$ . Since this isotope has a natural abundance of 0.01%, one of the dispensers (Alvac) contains potassium that is isotopically enriched to 7% with  $^{40}\text{K}$ . The dispensers are installed on a narrow 4.5 in. diameter spherical octagon (Kimball Physics) featuring 1.33 in. Conflat ports. Each one of the four dispensers is mounted on long copper wires supported with Groove Grabbers (Kimball Physics) attached to

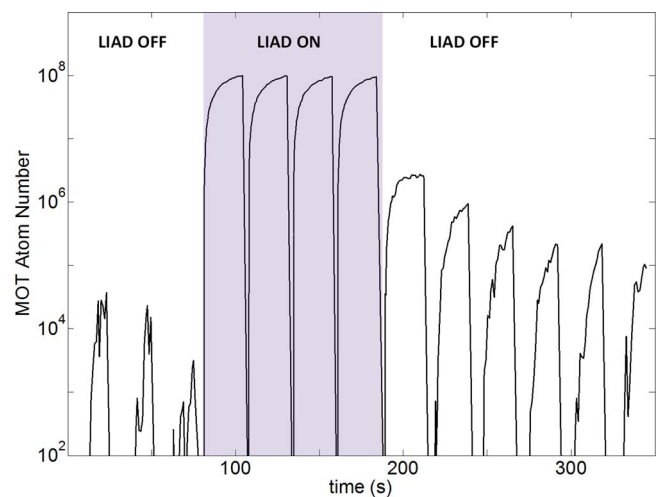


FIG. 2. LIAD assisted loading of the Rb MOT. Plot of MOT fluorescence versus time over the course of many 25 s loading periods. The shaded area shows when the LIAD light is on. The MOT fluorescence has been converted proportionally to an atom number based on an absorption imaging measurement of the MOT population. MOT populations several times larger are typical after activating the Rb dispenser for a few minutes.

the spherical octagon and connected to a 1.33 in. electrical feedthrough. The dispenser assembly is inserted into the MOT cell with the spherical octagon sandwiched between the 4.5 in. Conflat flange of the MOT cell and the six-way cube. The dispensers are positioned at the entrance of the rectangular part of the MOT cell.

We use light induced atom desorption (LIAD) to dynamically vary the Rb and K vapor pressure in the MOT cell by nearly three orders of magnitude on a sub-second timescale. We apply up to 1.8 W of 405 nm light from seven LED modules (Epitex, L405-66-60-550) during the MOT loading stage to desorb Rb and K atoms that were originally deposited on the cell walls by the dispensers: as Figure 2 shows, the LIAD process increases the Rb MOT population by up to a factor of  $10^4$ . In the case of  $^{39}\text{K}$ , we see increases in the MOT population of well over a factor of  $10^2$ . The LIAD light is turned off immediately after the MOT loading to allow the vacuum pressure to recover. The LIAD LEDs are powered by a lab-built constant current source.

## 4. Vacuum quality

The vacuum of the MOT cell is better than expected given that we activate a Rb dispenser (SAES) every one or two days for 5–10 min: We observe  $^{87}\text{Rb}$  MOT loading time constants on the order of 10 s and  $^{87}\text{Rb}$  and  $^{39}\text{K}$  magnetic trap lifetimes of about 18 s. We attribute this performance in part to our careful vacuum cleaning procedure.<sup>18</sup> The entire vacuum system was baked-out at 100 °C for two weeks.<sup>19</sup> The bake-out temperature is limited by the Alvac dispensers and UHV-grade electrically conductive epoxy used for connections to the atom chip. The lifetime of atoms in the chip trap is in the range of 7–9 s.

## B. Laser cooling system

The first cooling step towards producing a quantum gas is laser cooling in a large-beam collection MOT. As shown

in Figure 1, the MOT is formed by three pairs of counter-propagating beams directed into the MOT cell. We use large beams that are just under 5 cm in diameter to maximize the MOT loading rate.<sup>20,21</sup> The beams are not retro-reflected to minimize shadowing of the cooling beams and ensure a low laser cooling temperature.<sup>22</sup> We typically operate the MOT with a  $\sim 9$  G/cm magnetic gradient (strong axis) produced by anti-Helmholtz-style coils, which are also used for magnetic trapping. The MOT can cool both Rb and K isotopes simultaneously since the cooling light beams for both species are combined before being directed into the MOT cell. The laser-cooled atoms are monitored by their fluorescence with an industrial-grade CCD camera (Unibrain) placed directly above the MOT and a miniature TV camera. Once a sufficient number of atoms has been collected in the MOT, we extinguish the cooling light and the magnetic gradient, and then apply a brief (5–12 ms) optical molasses pulse to further cool the atoms down (30  $\mu$ K for  $^{87}$ Rb). The molasses pulse is followed by a short ( $\sim 1$  ms) optical pumping pulse before the atoms are loaded into the magnetic trap.

The Rb and K dual-species MOT is operated on the D2 lines of these elements at 780 nm and 767 nm, respectively. The K and Rb laser systems share a similar architecture (see Figure 3) for producing trap light and a somewhat lesser amount of repumper light for the dual species MOT, as well as

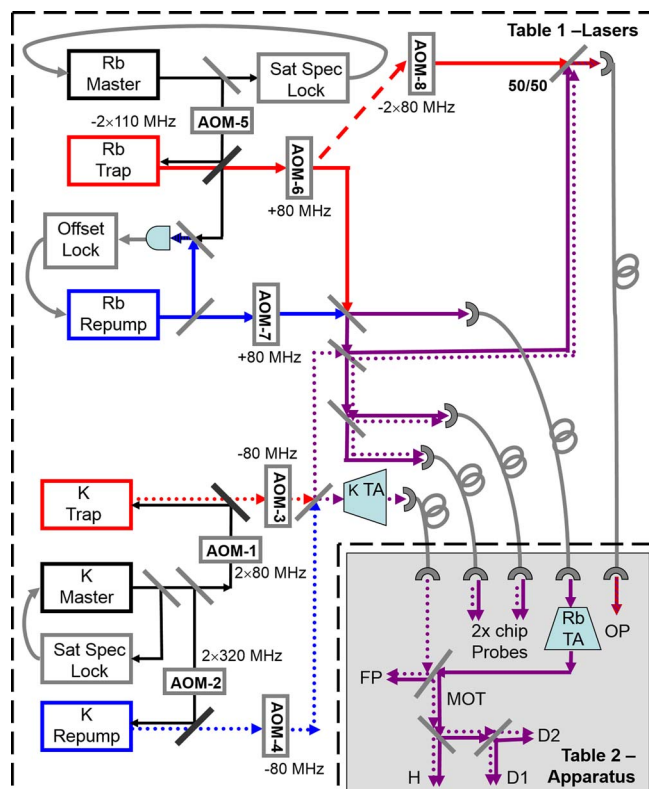


FIG. 3. Laser systems schematic for operating the MOT, optical pumping, and probe beams for Rb and K. Straight arrows represent free space laser beams. Curved gray arrows represent electrical signal. Gray lines with double loops represent optical fiber paths. TA: tapered amplifier. FP: Fabry-Perot cavity. OP: optical pumping and absorption probe for MOT cell. H, D1, and D2: Horizontal and diagonal trapping beams for MOT. The AOM frequencies indicate the nominal center frequencies of the devices. The representation is a schematic and does not reflect the actual layout of optical elements, laser beams, or optical tables.

probe light for imaging and optical pumping. A master external cavity diode laser (ECDL) is locked to a saturated absorption transmission line: we produce an error signal by using a lock-in amplifier to observe the saturated absorption probe signal at the roughly 100 kHz dither frequency of the pump light. The pump light frequency dither is inserted by way of a double-pass acousto-optic modulator (AOM) which imposes a frequency shift of  $+\nu$  on the pump light, but also causes the transmission line of the probe to be offset from the original saturated absorption transmission line by a frequency of  $-\nu/2$ .<sup>23</sup> Some master ECDL light is also sent through another double-pass AOM to injection lock a commercial diode laser via a Faraday rotator, thus providing a significant laser power increase. This second double-pass AOM provides frequency control of the injected laser light. The light from the injected laser is then sent through an 80 MHz single-pass AOM for amplitude control. The resulting light is then combined with another similarly generated beam to provide the trap and repumper light for the MOT. We also derive probe and optical pumping light by picking off light from the trap and repumper beams. Before being directed into optical fibers, these combined beams pass through lab-made optical shutters<sup>24</sup> to provide additional gating and optical path selectivity. Our scheme provides independent control between the trap (and probe) and repumper light, so that we can turn off the repumper light for absorption imaging, but turn it on for optical pumping and fluorescence imaging.

We amplify the combined trap and repumper light with a lab-built tapered amplifier setup<sup>25</sup> before sending it to the MOT. A shutter placed after the tapered amplifier blocks its spontaneous emission during magnetic trapping and transport. All lasers and tapered amplifiers are protected against back reflections with Faraday rotators.

The laser systems and the vacuum apparatus are on separate optics tables to suppress unwanted magnetic, electrical, optical, and mechanical coupling between these two systems. Optical fibers direct trapping light, laser probes, and optical pumping light onto the apparatus table.

The Rb and K trapping light is combined and then split up along six separate beams, which are then directed into the MOT via 1:5 expansion telescopes. We use dichroic waveplates ( $\lambda/2$  for 767 nm and  $\lambda$  for 780 nm) to independently control the power balancing for the Rb and K light along each arm of the MOT. A small portion of the combined Rb and K trapping light is picked off and sent to a commercial scanning Fabry-Perot cavity to monitor the individual powers of the trapping and repumper lasers for Rb and K simultaneously, while also verifying the proper injection locking of the lasers.

### 1. K lasers

The K laser system (see Figure 3) features a single 767 nm ECDL master laser (New Focus) locked to the  $^{39}\text{K}$   $4S_{1/2}, F = 2 \leftrightarrow 4P_{3/2}$  transitions. Following the earlier explanation of the laser lock scheme, the pump beam in the saturation spectroscopy setup is offset by  $\nu = +2 \times 90$  MHz with respect to the probe implying that the lock point of the ECDL is  $-\nu/2 = -90$  MHz from the transition line. We use master laser light to injection lock two different diode lasers

(Eagleyard EYP-RWL-0770-00025) simultaneously: one laser is offset by  $+2 \times 77.5$  MHz (AOM-1) and eventually serves as the trap laser, while the other is offset by  $+2 \times 310$  MHz (AOM-2) and eventually serves as the repumper. After subtracting 80 MHz from both beams with single-pass AOMs (AOM-3,4) and then combining them, we send a total of 15 mW to a tapered amplifier (Eagleyard EYP-TPA-0765-01500) to produce up to 90 mW of combined trapping and repumping light. We find that a 2:1 ratio of trap to repumper light is necessary for reliable operation of the  $^{39}\text{K}$  MOT. In principle, this architecture can be used for trapping  $^{40}\text{K}$  ( $^{41}\text{K}$ ) by replacing the 80 MHz double-pass AOM-1 used for the injection with a 320 MHz (110 MHz) AOM and locking the ECDL master laser to the  $^{39}\text{K}$  cross-over transition. A small fraction of the trapping and repumping light is picked off for use as probe and optical pumping light and then subsequently combined with the rubidium optical pumping and probe light; these beams are gated by mechanical shutters before being directed to the vacuum apparatus table via optical fibers.

## 2. Rb lasers

The Rb laser system consists of two ECDL lasers (New Focus) at 780 nm. One of the ECDL lasers (Rb Master in Figure 3) is locked to the  $5S_{1/2}$ ,  $F = 2 \leftrightarrow 5P_{3/2}$ ,  $F = 3$  saturated absorption line of  $^{87}\text{Rb}$ . As with the K laser lock scheme, we offset the pump beam so that the ECDL is locked +65 MHz above the transition line. We apply a  $-2 \times 110$  MHz frequency shift with a double-pass AOM (AOM-5) to the main output of the ECDL and use it to injection lock a diode laser (Sanyo DL7150-201W) with an output power of about 50 mW. This light is given a +80 MHz frequency shift (AOM-6) and serves as the trapping light after it is combined with repumper light from a second ECDL laser. While some of the combined beam power is used for absorption probes and optical pumping, most of the power is sent by fiber to a tapered amplifier (Eagleyard EYP-TPA-0780-01000) to provide 300 mW of usable power for the MOT. The Rb MOT laser beams have a typical peak intensity of  $1.4$  mW/cm<sup>2</sup> per beam. Alternatively, the laser system produces a  $^{85}\text{Rb}$  MOT when the master ECDL laser is locked instead to the  $5S_{1/2}$ ,  $F = 3 \leftrightarrow 5P_{3/2}$ ,  $F = 4$  saturated absorption line of  $^{85}\text{Rb}$ , and the reference lock frequency of the ECDL repumper laser, described in the next paragraph, is appropriately adjusted.

The Rb ECDL repumper laser is locked directly to the master ECDL laser frequency instead of an atomic transition. We combine a small amount of light with parallel polarizations from both ECDL lasers on a 50:50 beamsplitter and direct one of the resulting beams onto a low-cost, high-speed telecom photodiode (Finisar, HFD6180-418) to detect the beatnote between the two optical fields at about 6.4 GHz. The resulting microwave signal is converted to a digital pulse train with a limiting amplifier (Hittite, HMC750LP4). We use a divide-by-8 frequency divider (Hittite, MHC363G8) to reduce the signal below 1 GHz and then direct it to a phase-frequency detector (PFD) where it is compared to a 0.8 GHz reference signal. The PFD (Hittite, HMC439QS16G) generates an error

signal which we then feedback with a proportional-integral gain module to the piezo and current of the repumper ECDL laser to stabilize its frequency. This locking scheme is very robust (the laser rarely, if ever, needs to be re-locked, even in the presence of mechanical disturbances) and uses manufacturer-supplied evaluation boards for all the microwave and radio-frequency operations. The relative linewidth of the lock is comparable to the short term sub-MHz width of the beatnote when the ECDL lasers are free running. The repumper light is shifted by +80 MHz (AOM-7) before being combined with the trap light.

Finally, we generate optical pumping light on the  $5S_{1/2}$ ,  $F = 2 \leftrightarrow 5P_{3/2}$ ,  $F = 2$  transition by picking off light from the original trap injection laser beam and shifting it  $-2 \times 80$  MHz with a double-pass AOM (AOM-8) and combining it with some repumper light. We use this optical pumping light to preferentially populate the  $F = 2$ ,  $m_F = +2$  state after the optical molasses pulse to prepare the atoms for loading into the magnetic trap.

## C. Magnetic trapping system

Once collected and cooled in the MOT, the next step is to load the atoms into the magnetic trap in preparation for transport to the atom chip. As shown in Figure 4, we extinguish the MOT light, quickly turn off the MOT anti-Helmholtz coils (referred to as the “MOT coils”), and then apply optical molasses to further cool the atoms by turning the MOT light back on. Next, we apply a  $\sim 1$  ms optical pumping pulse to preferentially populate the  $F = 2$ ,  $m_F = 2$  state, and then quickly turn on the magnetic trap at 60 G/cm (strong axis) with 70 A

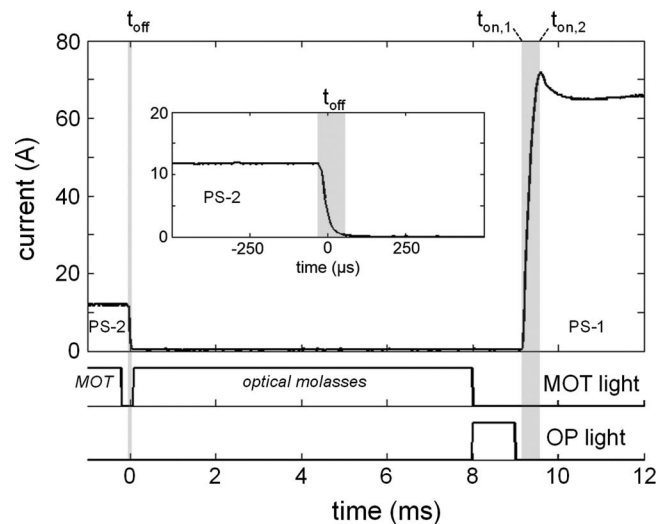


FIG. 4. MOT coils current switching for loading the magnetic trap. (Top) Plot of MOT coil current versus time for the MOT, fast turn-off, molasses, fast turn-on, and magnetic trap stages. The current was measured with an isolated current monitor (see Figure 5) and a low-pass filter (15  $\mu\text{s}$  time constant). The vertical gray bands show the times during which the “fast on” and “fast off” electronics are in operation (see Figure 5 and main text): power supply PS-2 provides the current before the “fast off” at time  $t_{\text{off}}$ , while power supply PS-1 serves as the current source after the “fast on” period, which starts and ends at times  $t_{\text{on},1}$  and  $t_{\text{on},2}$ , respectively. The inset shows a zoomed in view of the fast turn-off. (Bottom) Timing diagrams for the Rb MOT and molasses light and the Rb optical pumping (OP) light.

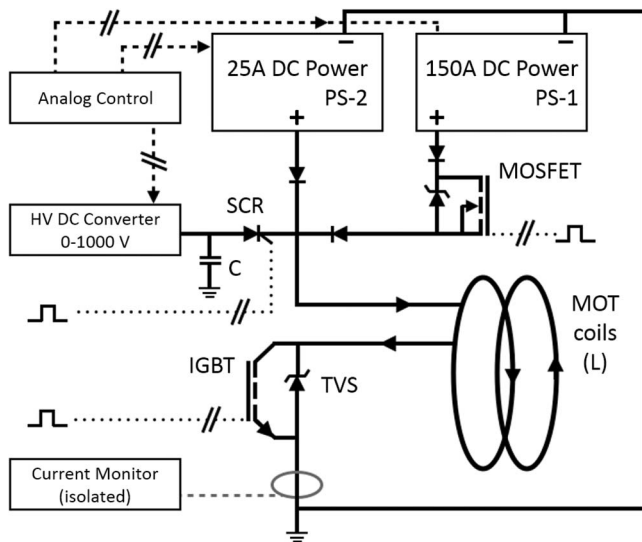


FIG. 5. Circuit used for rapid turn-on and turn-off of the MOT magnetic coils. The circuit ground is floating with respect to the main apparatus ground. All analog and digital control and monitoring signals are isolated: Optical digital isolation is represented by the  $\cdot \cdot / \cdot \cdot \cdot$  symbol, and analog galvanic isolation is represented by the  $- - / - -$  symbol. The IGBT symbol represents six such devices in parallel. The TVS symbol represents a stack of TVS diodes with a total clamping voltage of 1 kV. The MOSFET symbol represents two such devices in parallel. The SCR symbol represents a silicon-controlled rectifier diode.

in the MOT coils. The 30 G/cm vertical gradient is sufficient to overcome gravity for the  $F = 2$ ,  $m_F = 2$  state of  $^{87}\text{Rb}$ , but not for the  $F = 2$ ,  $m_F = 1$  state (both equivalent states of  $^{39}\text{K}$  can be trapped at this gradient), thus ensuring a spin-polarized  $^{87}\text{Rb}$  cloud. We do not employ this spin distillation method in  $^{39}\text{K}$ , since the optical pumping process is sufficiently efficient (due to the much smaller  $^{39}\text{K}$  MOT population relative to  $^{87}\text{Rb}$ ) for producing a magnetic trap of primarily  $F = 2$ ,  $m_F = 2$  atoms.

Each of the principal coils of the anti-Helmholtz MOT coils (circular purple coils in Figure 1) is composed of two single-layer copper ribbon wire coils and two insulated copper water cooling coils that form a wire-water-wire-water sandwich. We electrically connect the copper water coils in Helmholtz configuration to provide magnetic bias field trimming along the x-axis. The Helmholtz-style “push coils” (labeled P1 in Figure 1), used for transferring atoms from the magnetic trap to the transport system, are constructed in the same manner, but with single layers of ribbon wire and water cooling coils. Similarly, the water cooling coils from these are used for trimming the magnetic field along the z-axis. A small rectangular coil pair (purple in Figure 1) is used for vertical (y-axis) magnetic field adjustments.

We use a high current switch, shown in Figure 5, to control the current through the MOT coils for the MOT and magnetic trap. Despite the 0.6 mH inductance of the coils, the switch is capable of rapid turn-off from 100 A in less than 100  $\mu\text{s}$  (at time  $t_{\text{off}}$  in Figure 4) and fast turn-on to 70 A in under 400  $\mu\text{s}$  (between times  $t_{\text{on},1}$  and  $t_{\text{on},2}$  in Figure 4). The rapid turn-off is essential for maintaining the atomic cloud density prior to the molasses and enabling reliable absorption imaging of the MOT and magnetic trap. The fast turn-on

minimizes heating of the atoms during activation of the magnetic trap. The switch circuit is based on one from Ref. 26 but has been adapted to accommodate two power supplies. Our high current supply (Agilent, 6571A-J03, labeled PS-1 in Figure 5) cannot respond to programming changes faster than  $\sim 50$  ms, constraining the speed of magnetic field changes during the MOT to magnetic trap transition. We circumvent this limitation with a dual supply system that dedicates a modest current source (Kepco, ATE 6-25M, labeled PS-2 in Figure 5) to MOT operation, but switches in the PS-1 high current supply to run the magnetic trap. The pre-programmed PS-1 high current supply is connected via a high-current MOSFET switch (STMicroelectronics STV270N4F3) between the times  $t_{\text{off}}$  and  $t_{\text{on},1}$  of Figure 4); during this time we also set the voltage of power supply PS-2 to zero.

## 1. Fast off

We use a bank of six insulated gate bipolar transistors (IGBTs) in parallel as a high current switch to provide “fast off” and “fast on” operation of the MOT coils. At time  $t_{\text{off}}$  in Figure 4, the “fast off” electronics are triggered and break the circuit with the IGBTs, which causes a high voltage inductive spike  $\Delta V$  across the coils given by  $\Delta V = LdI/dt$ , with  $L$  and  $I$  the inductance and current of the coils: the faster the current is turned off, the higher the voltage spike. The IGBTs (International Rectifier, IRG4PSH71UDPbF) can tolerate a voltage of up to 1.2 kV when they block the current, so we clamp the spike at about 1 kV with a stack of high power transient voltage suppression (TVS) diodes. The PS-1 and PS-2 power supplies are each protected from voltage spikes and each other by power diodes with a reverse breakdown voltage in excess of 1.2 kV.

## 2. Fast on

The magnetic trap “fast on” requires the application of a large voltage to the MOT coils to drive the initial current increase. We use a  $C = 150 \mu\text{F}$  capacitor pre-charged to 180 V to act as a temporary high voltage source of high current. The PS-1 high current power supply is programmed as a voltage source and connected to the circuit with the MOSFET switch during the optical molasses stage. The pre-charged capacitor is kept behind a silicon-controlled rectifier (SCR) diode, which when triggered connects the capacitor to the circuit: 100  $\mu\text{s}$  after the SCR trigger, the IGBT switch is closed at time  $t_{\text{on},1}$  in Figure 4, and the capacitor quickly drives current through the MOT coils. The capacitor and MOT coils form a LC circuit with a  $f = 1/(2\pi\sqrt{LC})$  resonant frequency, and after a quarter period the current peaks at 70 A and the coil (and capacitor) voltage has dropped enough for the PS-1 high current supply to power the coils in constant voltage mode. At time  $t_{\text{on},2}$  in Figure 4, the SCR latches up and isolates the capacitor from the circuit so that the PS-1 high current supply becomes the only current source. The magnetic trap is held at 70 A for 500 ms to allow untrapped atomic states to fall away and to permit the power supply to transition to constant current mode. We then compress the trap to 80 G/cm (strong axis) for the transfer to the transport system.

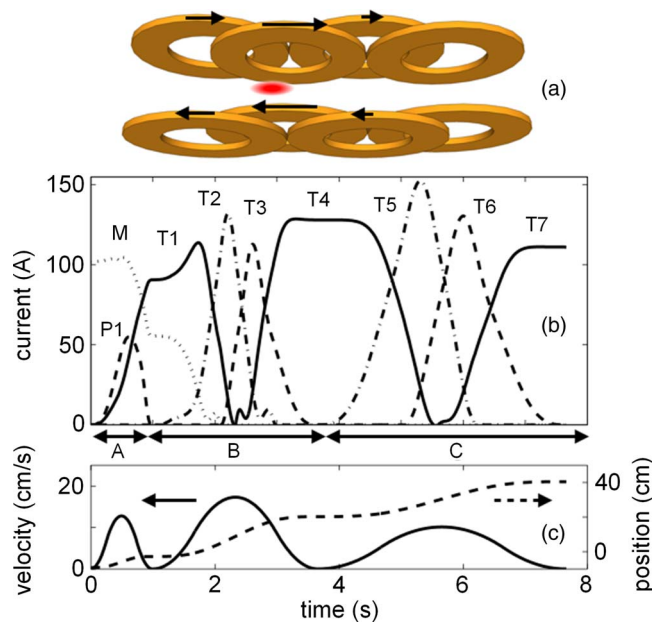


FIG. 6. Transport system operation. (a) Illustration of the 3-coil operation principle for adiabatic translation of trapped atoms (red). (b) Coil current sequence. M: magnetic trap current provided by power supply PS-1. P1: Push coil current (MOT cell). T1-7: Transport coil currents. The style of the current plot lines (dotted, dashed, solid, and dashed-dotted) represents which of four current sources is being used to power the labeled coil. The loading sequence from the coil T7 transport trap into the chip trap (using push coil P2 and the chip magnetic fields) is not shown. (c) Simulated velocity and position trajectories for the current sequence. (a) Magnetic trap to transport trap loading. (b) Transport to corner. (c) Transport from corner to atom chip region.

#### D. Magnetic transport system

We transfer the atoms from the MOT cell magnetic trap to the atom chip in the science cell with a transport system consisting of seven staggered quadrupole magnetic traps and no moving parts. Seven identical anti-Helmholtz coil pairs are interleaved over the 60 cm L-shaped path from the MOT to the atom chip: four from the MOT cell to the corner and three from the corner up to the science cell. The transport coil pairs overlap each other according to the arrangement shown in Figure 6(a). This scheme ensures that a magnetic quadrupole potential can be translated along the common weak axis of the coils by appropriately ramping the currents of three adjacent coil pairs.<sup>27</sup> A large Helmholtz-style push coil pair (labeled P1 in Figure 1), which produces a quasi-uniform magnetic field along the z-axis, assists the transfer of atoms from the magnetic trap into the first quadrupole trap of the transport system. Similarly, a single large water-cooled push coil (labeled P2 in Figure 1), positioned above the atom chip, produces a vertical magnetic field to assist with loading atoms into the micro-magnetic trap of the atom chip located 1.5 cm above the center of the final transport coil pair.

The current ramps (see Figure 6(b)) necessary for transporting the atoms by adiabatic translation, with minimal heating are determined by meeting three conditions:<sup>28</sup> (1) The total magnetic field at the (moving) trap center must be zero; (2) the gradient along the translation axis must remain fixed; and (3) the aspect ratio between the two orthogonal axes must remain fixed at an optimal value determined by the coil geometry. These conditions are maintained by using three pairs of

coils simultaneously and using a predetermined position and velocity curve (see Figure 6(c)) to generate the current ramping sequence displayed in Figure 6(b). The overall timing is scaled experimentally to maximize speed and efficiency while minimizing heating of the atomic cloud.

#### 1. Transport coils

Each of the transport coil pairs consists of two 26-turn coils of copper ribbon wire. These coils are mounted to a water-cooled copper and thermoplastic heatsink frame to dissipate up to 1.5 kW of peak power consumed by the coil pairs. We use thermal epoxy (Epoxies etc., 50-3170BK) to bond the coils to the heatsinking frame. Thermoplastic is used for the first and last coils to minimize the risk of eddy currents in the vicinity of the MOT and the atom chip. The transport current ramps of Figure 6(b) are too slow to produce any significant eddy currents.

#### 2. Current multiplexer

Since the transport system only requires three or fewer coils to be under current at once, we power it with three power supplies (Agilent, 6571A-J03) that are multiplexed to the seven transport coil pairs and the two push coils. As shown in Figure 7, each power supply is connected to three transport system coil pairs whose current can be turned on or off by means of a MOSFET-based high current switch (two STV270N4F3 in parallel). A 2-bit selector guarantees that only a single switch of the three can be on at any one time. During the course of the transport system current ramps,

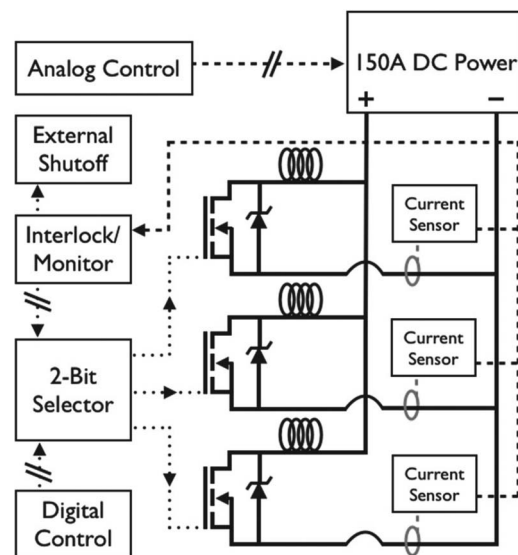


FIG. 7. Current multiplexer circuit for the transport system. The circuit directs up to 150 A of current from a high current power supply to one of three transport coils based on a 2-bit digital control signal. A fourth back-up output is not shown. Three such circuits allow three power supplies to direct current to the seven transport coils and two push coils. The MOSFET symbol represents two such devices in parallel. The TVS symbol represents six such devices in parallel with a 15 V clamping voltage. Optical digital isolation is represented by the  $\cdot \cdot \cdot \cdot$  symbol, and analog galvanic isolation is represented by the  $- \cdot \cdot \cdot -$  symbol.

shown in Figure 6(b), the multiplexer switches from one coil to another when the current is brought to zero. A bank of six bi-directional TVS diodes protects each MOSFET switch and its power supply against the inductive voltage spike produced by switching a coil in the event that it has not been powered down. Moreover, these protection diodes also ensure a sub-millisecond turn-off time for each fully powered coil pair. All digital control lines feature optical isolation to limit the possibility of ground loops. Furthermore, due to the high currents involved, the transport system is fully isolated from the apparatus ground: The analog control lines for the high current power supplies are attached to the main sequencer via galvanic isolation buffers (Texas Instruments, ISO124); the MOSFET switches are powered by floating DC-DC voltage regulators; and the coils are electrically isolated from their heat sink frame.

While the transport system is thoroughly heat sunk and water cooled, the coils dissipate sufficient power that thermal damage remains a danger. As depicted in Figure 7, the multiplexer circuit includes isolated current sensors for each coil pair that are monitored by a safety-interlock circuit. This safety system imposes a global maximum current threshold as well as local and global current-time integration thresholds. If any of these preset thresholds are crossed, the system will fault, turning off all the MOSFET switches. As an added precaution a trip signal is also sent to an external safety-interlock system that monitors the temperatures of the transport system and other apparatus coils. When this external protection system detects an over-current or over-temperature condition, it turns off all the high current power supplies via solid state relays installed on the AC power lines for these devices.

### E. Atom chip

The atom chip is the primary location for experiments. As such, it features a number of DC and RF magnetic fields for producing a micro-magnetic trap for RF evaporation to quantum degeneracy, as well as for future experiments. Additionally, the atom chip has several optical probes and imaging systems directed at it for *in situ* and time-of-flight measurements. The tight confinement of the chip trap ensures fast re-thermalization times for rapid RF evaporation. The atom chip is well suited for experiments requiring highly elongated or pseudo-1D traps, RF near-field potentials, or a nearby surface for atom-surface force studies. Generally, a new experiment requires only a modification to the atom chip and not the entire apparatus.

In order to produce a BEC, the atoms are confined in the Z-wire trap produced by a thin Z-shaped wire on the chip, as shown in Figure 8. The central portion of the wire is 50  $\mu\text{m}$  wide, while the “endcap” leads are 200  $\mu\text{m}$  wide. The wire has a thickness of just over 3  $\mu\text{m}$ . A cigar-shaped Ioffe-Pritchard style trap is produced below the Z-wire, when a DC current is directed through it in combination with the application of an external bias magnetic field  $B_{hold}$ , parallel to the plane of the chip and transverse to the central portion. The “endcap” leads ensure that the trap minimum occurs at non-zero magnetic field, and we add a longitudinal magnetic

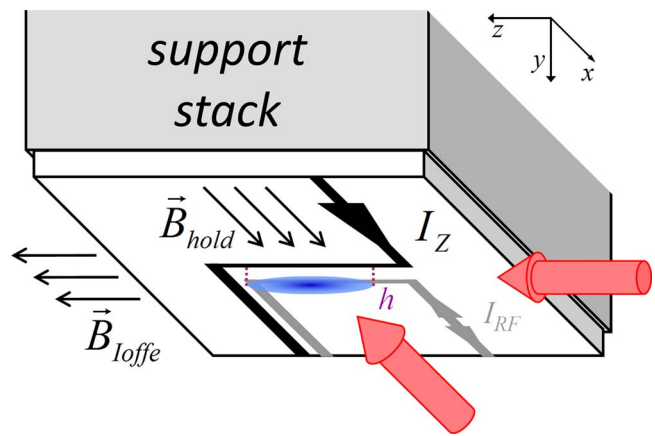


FIG. 8. Atom chip Z-wire trap schematic. The magnetic field of the Z-wire current  $I_Z$  and the external bias magnetic field  $B_{hold}$  generate a cigar-shaped Ioffe-Pritchard style trap, represented by the blue cloud, at a distance  $h$  below the central Z-wire segment.  $B_{loffe}$  is directed along the long axis of the trap and sets the magnetic field at the bottom of the trap. The red arrows indicate absorption imaging lasers. While the representation is not to scale, the coordinate system matches the one in Figure 1.

field  $B_{loffe}$ , parallel to the central wire, to increase this magnetic minimum. The trap is harmonic in all directions: for a wire current  $I_Z = 1$  A,  $B_{hold} = 20$  G, and  $B_{loffe} = 4.9$  G, the calculated axial and radial trap frequencies for Rb (K) are  $\omega_z = 2\pi \times 9.3$  Hz ( $2\pi \times 13.9$  Hz) and  $\omega_r = 2\pi \times 1.1$  kHz ( $2\pi \times 1.6$  kHz), respectively; the trap is 100  $\mu\text{m}$  from the chip surface. We use a U-shaped wire to produce a RF magnetic field in the 1–20 MHz range for forced evaporation of chip-trapped atoms. In addition to the U and Z wires, the atom chip features a number of additional wire structures for future manipulation of the trapped atoms with magnetic biases, gradients, and RF fields that are not shown in Figure 8.

The chip is connected by screws at its corners to an aluminum support stack, which is mounted on a vacuum flange above it. This stack serves as heat sink for power dissipated in the chip wires and as support for the wire leads that feed the chip. A small amount of vacuum compatible epoxy (model: FO-EPXY-UHV, Accu-Glass Products, Inc.) bonds the chip to the stack for improved thermal conductivity. The support stack is attached to a multiport flange that provides DC and RF (SMA) electrical connections. Kapton-insulated wires and coaxial cables connect the electrical feedthrough to the chip. These wires are attached to the chip with vacuum-compatible electrically conductive epoxy (EPO-TEK H21D, Epoxy Technology, Inc.).

The Z-wire trap is powered by a fast, high stability, precision bipolar current source (High Finesse, BCS 5/5). In order to suppress noise and ground loops, the current source is galvanically isolated from the analog control signal ground. One side of the chip wire is explicitly grounded to the optics table and the multiport vacuum flange. An over-current protection interlock system ensures that the Z-wire current  $I_Z$  remains at or below 1 A for at most 10 s, which we have determined to be safe based on resistive heating measurements. Two compact Helmholtz-style coil pairs (blue in Figure 1), positioned a few millimeters from the science cell and centered on the chip, provide a holding field  $B_{hold}$  along the x-axis and a Ioffe

field  $B_{\text{offe}}$  along the  $z$ -axis, as shown in Figure 8. A single horizontal coil (also blue in Figure 1) above the chip provides a modest vertical bias magnetic field. These three bias coils are powered by high speed bipolar current sources (Kepco BOP series) for rapid modulation and turn-off on time scales of 100–200  $\mu\text{s}$ .

The U-wire RF current is produced by a custom RF circuit. A 16 dBm RF signal is generated by a direct digital synthesis function generator (Berkeley Nucleonics, model 645). We control the RF amplitude with an analog voltage controlled attenuator and a TTL RF switch. The RF signal is sent to the chip via an isolation transformer and a series 50  $\Omega$  resistance for impedance matching. Forced evaporation frequency sweeps are produced by frequency modulating the RF source with an analog ramp signal.<sup>29</sup> A RF amplifier is not necessary due to the proximity of the atoms to the U-wire.

## F. Imaging systems

We use absorption imaging for *in situ* and time-of-flight measurements of atomic cloud parameters, such as density, temperature, and atom number. As shown in Figure 8, probe lasers are directed parallel to the chip along the axial and horizontal radial axes to image the atoms with CCD cameras. We employ industrial grade cameras (Unibrain, Fire-i 530b and Fire-i 701b) with the CCD chip cover glass removed to avoid interference fringes from it. The cameras are each fitted with a 1:1 achromatic doublet pair imaging system (Thorlabs, MAP10100100-B) with a 10 cm imaging distance. While these probe lasers can be used for fluorescence imaging of very small atomic clouds, we generally use absorption imaging for high fidelity measurements of atomic cloud parameters. We employ a double-shot imaging method whereby 0.3–0.5 s after taking an image with atoms present, a reference image is taken without the atoms, so as to minimize non-atomic variations in between the imaging and reference probe pulses.

Despite using Gaussian laser probes from a single mode polarization maintaining fiber, we find that the probes that impinge upon the CCDs contain several interference fringe patterns. The glass cell presents four non-anti-reflection coated surfaces, and we see interference fringes due to these, though they are quite stable over the double-shot imaging duration. Experimentally, we find that reflections between the imaging systems and other optical elements in the absorption probes' paths, such as the glass cell, produce high-frequency interference fringes that are not stable over the course of the double-shot period. However, careful adjustment of the imaging systems' orientation and position can minimize these fringes sufficiently.

We monitor the MOT with a top view CCD camera similar to those used for the atom chip. The camera is used for aligning the MOT with the magnetic trap and for temperature measurements of the cold atoms. This CCD camera can also be used for absorption imaging of MOT-region atoms using resonant light directed along the optical pumping laser path with which it is aligned. We also use a black and white TV camera for general monitoring of the MOT.

## G. Optical dipole traps

The apparatus includes two optical dipole traps: a low power trap in the vicinity of the atom chip, and a high power crossed dipole trap in the MOT cell.

The chip dipole trap is based on a 1.5 W 1064 nm fiber laser (NovaWave Technologies). We use about 1 W of optical power, controlled by an 80 MHz AOM, to form the trap. The output power of the laser is sufficiently stable that no active power stabilization is necessary. The chip dipole trap has an estimated trap depth of 20  $\mu\text{K}$ <sup>30</sup> for a 60  $\mu\text{m}$  waist and is aligned with the main axis of the Z-wire trap for approximate mode-matched transfer between them. Conveniently, a  $\lambda/2$  waveplate and a polarizing beamsplitter cube can be used to direct the dipole trap light at the chip region or the MOT cell.

The crossed-dipole trap in the MOT cell is formed by two lasers: a 10 W 1064 nm Nd:YAG laser (Spectra-Physics, model 3800) and light re-directed from the 1064 nm fiber laser. We use about 6 W of the Nd:YAG light, controlled by a high-power 40 MHz AOM, for the dipole trap. We actively stabilize the Nd:YAG laser power to better than  $\pm 0.6\%$  (peak-to-peak) over a bandwidth of 10 kHz. We use a 30 cm achromat lens to focus the Nd:YAG laser down to a somewhat elliptical waist with a mean radius of 120  $\mu\text{m}$  to form a dipole trap. We form a crossed dipole trap by folding the trapping beam back on itself through a second 30 cm lens, but with a small angle between the two beams. The broadband nature of the laser and the 1.4 m distance over which the laser is folded back on itself combine to partially suppress the formation of an optical lattice at the trap: Based on first-order coherence measurements, we estimate the lattice fringes to be on the order of 20% or less of the total trap laser intensity and are working on additional mechanisms to further suppress these. In the limit of no lattice fringes, the trap has an estimated depth of 50  $\mu\text{K}$ .<sup>30</sup> Optionally, we focus the 1064 nm fiber laser light with another 30 cm achromat lens onto the Nd:YAG trap to form a tighter crossed dipole trap. All of the dipole laser beams are directed horizontally into the MOT cell at small angles from the two horizontal MOT beams.

## III. PERFORMANCE

The apparatus functions as designed and, at present, produces quasi-pure BECs with a 40 s cycle time. We focus first on the performance of the apparatus from MOT to BEC on the chip for <sup>87</sup>Rb (Subsection III A). In Subsection III B, we present details on the dimple in our Z-wire chip trap. Finally in Subsections III C and III D, we describe on-going work with potassium and the dipole traps, respectively.

### A. Rubidium: MOT to BEC

The MOT collects several  $10^8$  <sup>87</sup>Rb atoms in 25 s at a temperature of about 60  $\mu\text{K}$  with a detuning of 21 MHz  $\approx 3.5\Gamma$  and a peak intensity per beam of  $1.4 \text{ mW/cm}^2 \approx 0.8I_{\text{sat}}$ ;  $\Gamma$  and  $I_{\text{sat}}$  are the linewidth and saturation intensity for the  $D_2$  cycling transition. After turning off the MOT light and

magnetic gradient, we apply a 5–12 ms molasses stage by turning the MOT light back on at reduced power and a detuning of 56 MHz  $\approx 9.2\Gamma$  with the repumping power reduced. As shown in Figure 4, we then apply a 1.1 ms optical pumping pulse to preferentially populate the  $F = 2, m_F = 2$  ground state and load up to  $3 \times 10^8$  into the magnetic trap (80 G/cm). At this point the atoms have a temperature of about 50  $\mu\text{K}$ , a phase-space density (PSD) of  $2 \times 10^{-6}$ , and a collision rate of  $6 \text{ s}^{-1}$ . The atoms are then transferred to the transport system, which conveys them around the corner and up to the atom chip in the science cell in just under 8 s.

We load over  $5 \times 10^6$   $^{87}\text{Rb}$  atoms into the chip Z-wire trap by adiabatically ramping up the Z-wire current to  $I_Z = 1$  A and the holding magnetic field to  $B_{\text{hold}} = 20$  G while slowly turning off the transport quadrupole trap over the course of 450 ms. We also apply an axial magnetic field  $B_{\text{offe}} = 4.9$  G to protect against spin-flip loss from low-frequency RF noise. Once the atoms are fully loaded into the chip trap, the PSD is  $5 \times 10^{-6}$  with a peak collision rate of at least  $30 \text{ s}^{-1}$  per atom. We observe a chip trap lifetime of about 7 s. Next, we compress the atoms to increase the collision rate by ramping up the holding field to  $B_{\text{hold}} = 46.4$  G, resulting in a radial trapping frequency (calculated)  $\omega_r = 2\pi \times 4.5$  kHz. The compression occurs over 1 s and results in some evaporation, yielding a PSD of  $8 \times 10^{-6}$  with  $4 - 5 \times 10^6$  atoms. We turn on the RF evaporation knife produced by the U-wire current  $I_{\text{RF}}$  at 19 MHz during the chip loading and begin to ramp it down after the compression. After reaching a PSD of  $10^{-2}$  with  $3 \times 10^5$  atoms, we relax the chip trap by ramping down  $B_{\text{hold}}$  to 20 G to produce a more relaxed trap 100  $\mu\text{m}$  (calculated) from the chip. We perform the final evaporation to BEC in the relaxed trap by ramping the RF knife from 3.8 MHz down to 3.4 MHz over the course of 2 s, with the final 50 kHz covered in 0.8 s. Figure 9 shows the PSD as a function of atom number for the evaporative cooling path for  $^{87}\text{Rb}$  in the Z-wire trap. The entire evaporation process takes 6 s from compression to BEC.

We observe the BEC transition at  $T \sim 0.3 \mu\text{K}$  with  $2 - 4 \times 10^4$  atoms and produce quasi-pure BECs with  $10^4$  atoms. In

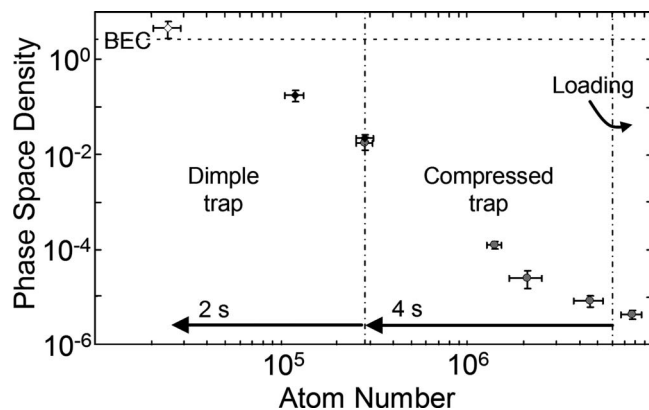


FIG. 9. Evaporative cooling path to  $^{87}\text{Rb}$  BEC in the Z-wire trap. Plot of phase-space density versus atom number from the initial loading into the Z-wire trap, through 4 s of RF evaporation in the compressed trap, to the final 2 s of RF evaporation in the dimple trap to quantum degeneracy. The final point above the threshold for BEC has been obtained using the same semi-classical definition for PSD as the other points.

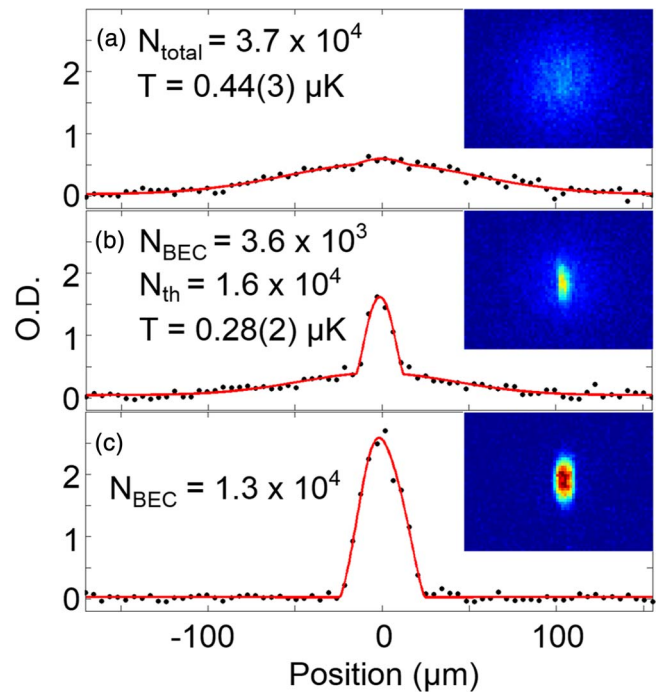


FIG. 10. Bose-Einstein condensation of  $^{87}\text{Rb}$ . Optical density cross-sections plots and related absorption images of (a) thermal atoms, (b) partially condensed atoms, and (c) a quasi-pure BEC for a time-of-flight of 8.45 ms after release from the chip trap. The inset images of the BEC show the inversion of the trap aspect ratio, while the thermal cloud has an isotropic momentum distribution. The cross-section plots show the bi-modal distribution of the atomic momenta as the BEC emerges from the thermal Gaussian cloud. The red line is a bi-modal fit using Gaussian and Thomas-Fermi distributions integrated along the optical probe axis (x-axis).

Figure 10, we show the onset of BEC through the appearance of the bi-modal distribution of the BEC peak on top of the Gaussian thermal cloud and the inversion of the BEC aspect ratio during the TOF expansion.

## B. Dimple trap

Atom chip micro-magnetic traps frequently exhibit potential roughness, and our Z-wire trap is no exception. Evaporation in the compressed trap quickly loses efficiency at temperatures below 3  $\mu\text{K}$  (this is the temperature after decompression to the relaxed trap used for imaging, according to the trap parameters listed in Sec. II E). Figure 11(a) shows an image of 3.4  $\mu\text{K}$  cloud of  $^{87}\text{Rb}$  atoms, at very short TOF after turn off of the Z-wire trap, which shows the appearance of faint clumping in the atomic density distribution. We attribute these density irregularities to potential roughness, which can create small localized potential wells, or dimples, in the axial trapping potential. These irregularities impede thermalization in the axial direction and can lead to heating when the trap is decompressed. As shown in Figure 11(c), we apply a modest magnetic gradient along the Z-axis of the trap with the last quadrupole coil pair of the transport system to center the atomic cloud on the largest dimple. We perform this action at the end of the compressed trap stage and find that it is sufficient to push most of the atoms into this dimple. While the dimple is a little under 2  $\mu\text{K}$  deep, it benefits from a

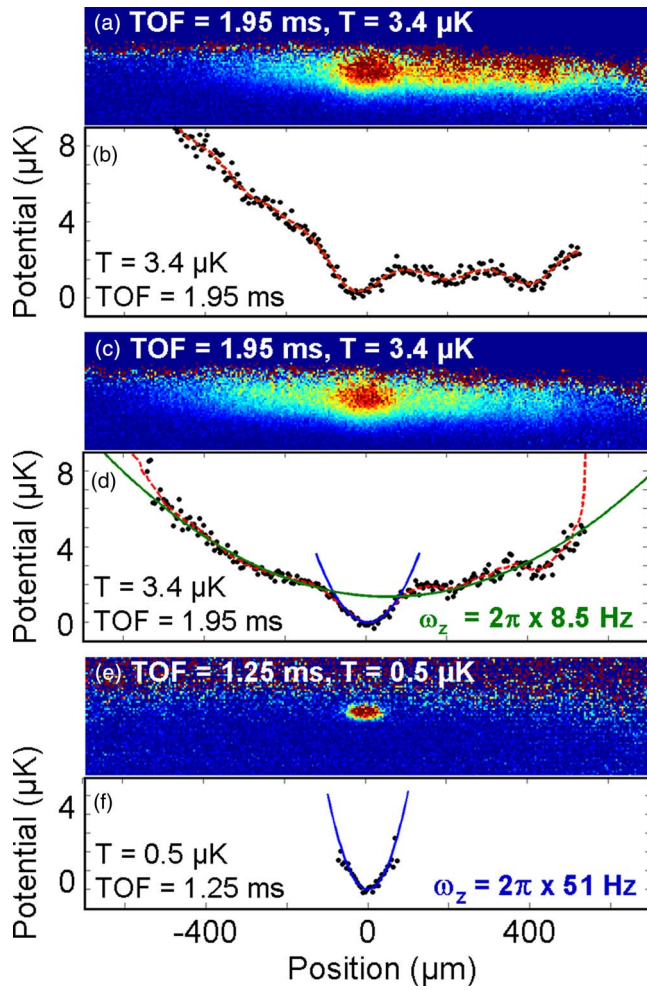


FIG. 11. Axial Z-wire dimple potential using *in situ* imaging of  $^{87}\text{Rb}$  atoms. (a) Absorption image of atoms at  $3.4\ \mu\text{K}$  from the Z-wire trap showing clumping in the main dimple along with fainter clumping in dimples on the right. (b) Axial trapping potential derived from image in (a) showing multiple dimples; the dashed red line is a running average of the trapping potential. (c) Absorption image of  $3.4\ \mu\text{K}$  atoms from the Z-wire trap after centering on the main dimple. (d) Axial trapping potential derived from image in (c); the dashed red line is a running average of the trapping potential, while the green and blue parabolas are least-squares fits to the overall and dimple trapping potentials, respectively. (e) Absorption image of  $0.5\ \mu\text{K}$  atoms in the main dimple. (f) Dimple potential derived from image in (e) and parabolic fit (blue). The  $\omega_z$  values listed in (d) and (f) refer to the axial trapping frequencies obtained from the green and blue parabolic fits, respectively.

relatively high axial trapping frequency: we measure the axial and radial trapping frequencies of the dimple to be  $\omega_z = 2\pi \times 53\ \text{Hz}$  and  $\omega_r = 2\pi \times 1.04\ \text{kHz}$ , respectively, by observing axial and radial oscillations of excited clouds. The final evaporation then benefits from enhanced rethermalization due to the tight axial confinement of the dimple.

We determine the axial potential directly by *in situ* imaging of ultracold  $^{87}\text{Rb}$  atoms at very short TOF. The in-trap density is approximately given by  $n(\vec{r}) \simeq \exp[-U(\vec{r})/kT]/\Lambda^3$ , where  $U(\vec{r})$  is the trapping potential,  $\Lambda = h/\sqrt{2\pi M k T}$  is the thermal deBroglie wavelength,  $T$  is the temperature of the gas,  $k$  is Boltzmann's constant,  $h$  is Planck's constant, and  $M$  is the mass of the gas particles.<sup>14,31</sup> In Figures 11(b) and 11(d), we show the axial potentials derived from the  $T = 3.4\ \mu\text{K}$  images at 1.95 ms TOF in

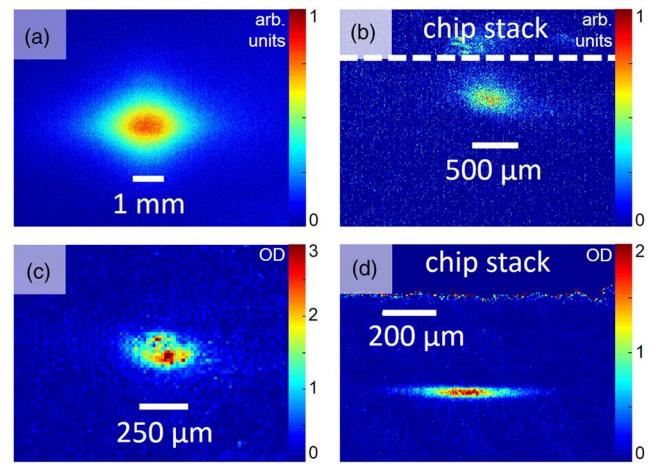


FIG. 12. False color images of the potassium magnetic traps and rubidium dipole traps. (a) Fluorescence image of the  $^{39}\text{K}$  MOT cell magnetic trap with about  $6 \times 10^6$  atoms. (b) 1D MOT fluorescence imaging of roughly  $6 \times 10^3$   $^{39}\text{K}$  atoms in the chip Z-wire trap. The dashed line indicates the atom chip. (c) Absorption image of about  $3 \times 10^6$   $^{87}\text{Rb}$  atoms in the MOT cell 1064 nm dipole trap (6 W retro-reflected) loaded from the magnetic trap. (d) Absorption image of about  $6 \times 10^4$   $^{87}\text{Rb}$  atoms in the dipole trap located near the chip. The colorbars for the absorption images ((c) and (d)) are in units of optical depth (OD), while those for the fluorescence images ((a) and (b)) are in arbitrary units.

Figures 11(a) and 11(c), respectively, after summing over the radial distribution: ignoring the dimples, the overall axial trapping potential in Figure 11(d) is basically harmonic with an inferred axial frequency of  $\omega_z = 2\pi \times 8.5\ \text{Hz}$ . At this temperature and TOF, the potential of the dimple is blurred by the motion of the expanding atomic cloud. We obtain a better representation of the axial potential by reducing the temperature to  $T = 0.5\ \mu\text{K}$  at 1.25 ms TOF: As shown in Figures 11(e) and 11(f), there remains some blurring, but the resulting axial trapping frequency  $\omega_z = 2\pi \times 51\ \text{Hz}$ , which was obtained from a parabolic fit of the potential, approaches the oscillation-based measurement.

### C. Potassium: Cooling and trapping

We have laser cooled a sample of  $^{39}\text{K}$  atoms, loaded them into the magnetic trap (see Figure 12(a)), transported them to the atom chip, and successfully loaded them into the Z-wire trap (see Figure 12(b)). We operate the potassium MOT in two stages<sup>32</sup> (see Table I for details): a collection stage (KMOT)

TABLE I. Table of  $^{39}\text{K}$  laser cooling parameters. The trap and repumper lasers are operated on the  $4S_{1/2}, F \leftrightarrow 4P_{3/2}, F'$  transitions, and their respective detunings,  $\delta_t$  on  $F = 2 \leftrightarrow F' = 3$  and  $\delta_r$  on  $F = 1 \leftrightarrow F' = 2$ , are given in units of the transition linewidth  $\Gamma = 6.1\ \text{MHz}$ . The total peak laser intensity  $I_{tot} = I_t + I_r$  (summed over all MOT beams) is given in units of the saturation intensity  $I_{sat} = 1.8\ \text{mW/cm}^2$ .

Stage	Time	$\delta_t$	$\delta_r$	$I_{tot}$	$I_t : I_r$	T ( $\mu\text{K}$ )
KMOT	10–30 s	−2.8	−3.6	18	2:1	>1000
CMOT	0.1 s ramp	−0.8	−3.6	11	12:1	$\lesssim 70$
1D MOT	20 ms	−2.1	−3.3	10	2:1	...

uses far-detuned trapping light to maximize the number of trapped atoms, after which a short stage of near-detuned trapping light further cools and compresses the atoms (CMOT) for loading into the magnetic trap. Both MOT stages use a magnetic gradient of 8 G/cm.

After fast turn-off of the MOT coils, we use a 1.5 ms optical pumping pulse to preferentially populate the  $|F = 2, m_F = +2\rangle$  state and then quickly load the atoms into the magnetic trap. Once in the magnetic trap (60 G/cm), the atoms have a temperature of about 60  $\mu$ K. The atoms are then transferred to the transport system, delivered to the chip region, and then loaded into the chip Z-wire trap using the  $^{87}\text{Rb}$  procedure. Successful chip loading requires low temperatures and large atom numbers: The image in Figure 12(b) was obtained with a large  $^{39}\text{K}$  MOT enabled by increasing the total MOT trapping power to 200 mW by sending the light from the K tapered amplifier into the Rb tapered amplifier for further amplification. Figure 12(a) shows the magnetic trap produced by this double amplifier method. We observe a Z-wire trap lifetime of about 9 s for  $^{39}\text{K}$ , comparable to the  $^{87}\text{Rb}$  lifetime. We have also applied the cooling, trapping, and transport procedure to both Rb and K simultaneously, in anticipation of future sympathetic cooling of K by Rb.<sup>33</sup> In the future, we plan to convert the potassium tapered amplifier to a double-pass configuration<sup>34</sup> to maximize the available trapping power and produce larger ultracold potassium samples.<sup>35</sup>

Due to the smaller K atom numbers relative to Rb, we image the atoms in the chip trap by applying a circularly polarized, retro-reflected, red-detuned probe laser along one of the absorption imaging paths and observing the fluorescence with the camera transverse to the beam (see Figure 12(b)). We refer to this method as “1D MOT” imaging<sup>26</sup> (see Table I for laser parameters), since the setup mimics a MOT with two counter-propagating trapping beams and a magnetic field minimum provided by the Z-wire trap ( $I_Z = 1$  A,  $B_{\text{hold}} = 11.6$  G,  $B_{\text{loffe}} = 2.5$  G).

#### D. Dipole traps

We operate separate dipole traps in the MOT cell and at the atom chip. We have successfully loaded near-degenerate thermal  $^{87}\text{Rb}$  atoms from the Z-wire trap into the atom chip dipole trap (see Figure 12(d)), which we are using for experiments in the vicinity of the atom chip.<sup>36</sup> In the MOT cell, we have successfully loaded atoms into the crossed dipole trap (see Figure 12(c)) from the magnetic trap by operating both traps simultaneously and performing RF evaporative cooling, following the method of reference:<sup>14</sup> we obtain a phase space density of  $10^{-4}$  with up to  $6 \times 10^6$   $^{87}\text{Rb}$  at  $\mu$ K-level temperatures and a 14 s lifetime in the retro-reflected 6 W dipole trap. We are optimizing the alignment of the crossed dipole trap lasers in preparation for evaporative cooling to higher phase space densities by lowering the trapping laser intensities.

#### IV. CONCLUSION

In conclusion, we have constructed a dual-species ultracold atom apparatus that combines several innovations, such

as LIAD, magnetic transport, optical trapping in two chambers, and an atom chip. The apparatus produces  $^{87}\text{Rb}$  BEC in an atom chip micro-magnetic trap. We have also laser cooled  $^{39}\text{K}$  atoms and transported them to the second chamber, and then loaded them into the chip Z-wire trap: to our knowledge this experimental milestone is the first time that bosonic potassium has been confined in a chip trap, opening up the possibility of a chip-based ultracold gas or BEC with tunable interactions via low-field Feshbach resonances. Furthermore, the vacuum in the MOT cell is sufficiently good to support dipole trap-based experiments, thus roughly doubling the viable locations for experiments on the apparatus. The next step in preparing the  $^{39}\text{K}$  atoms for experiments is to cool them to  $\mu$ K-range temperatures or lower via sympathetic cooling by  $^{87}\text{Rb}$ ,<sup>37</sup> which is necessary due to the limited number of trapped  $^{39}\text{K}$  atoms. In principle, the methods presented here can be extended to trapping bosonic  $^{41}\text{K}$ ,  $^{85}\text{Rb}$ , or fermionic  $^{40}\text{K}$  on the chip.

The separation of the vapor-loaded MOT and the atom chip into two distinct vacuum chambers prevents line-of-sight contamination of the atom chip region. This feature ensures that substrate surfaces near the atom chip will remain relatively clean for future atom-based surface studies, such as measurements of the Casimir-Polder force. We envisage using the low magnetic field Feshbach resonances of the bosonic potassium isotopes to enhance or suppress inter-atom interactions for atom interferometry and many-body physics experiments. The apparatus is also well suited for other planned atom chip-based experiments, such as tests of novel trapping schemes using RF near-fields and studies of quantum pumping and transport.<sup>36</sup>

#### ACKNOWLEDGMENTS

This work was supported by the College of William and Mary, the Jeffress Memorial Trust, and the Virginia Space Grant Consortium (VSGC). M.K.I., A.R.Z., and C.F. acknowledge support from VSGC. We thank C. Sukenik (Department of Physics, Old Dominion University) for the long-term loan of the Spectra-Physics 3800 laser, S. Schmidt for experimental assistance with the K tapered amplifier, and E. Urbach and I. Lee for help with the MOT cell dipole trap.

- <sup>1</sup>I. Bloch, J. Dalibard, and W. Zwerger, *Rev. Mod. Phys.* **80**, 885 (2008).
- <sup>2</sup>A. D. Cronin, J. Schmiedmayer, and D. E. Pritchard, *Rev. Mod. Phys.* **81**, 1051 (2009).
- <sup>3</sup>M. A. Kasevich, *Science* **298**, 1363 (2002).
- <sup>4</sup>J. Fortágh and C. Zimmermann, *Rev. Mod. Phys.* **79**, 235 (2007).
- <sup>5</sup>T. Schumm, S. Hofferberth, L. M. Andersson, S. Wildermuth, S. Groth, I. Bar-Joseph, J. Schmiedmayer, and P. Krüger, *Nat. Phys.* **1**, 57 (2005).
- <sup>6</sup>W. Mainault, C. Deutsch, K. Gibble, J. Reichel, and P. Rosenbusch, *Phys. Rev. Lett.* **109**, 020407 (2012).
- <sup>7</sup>P. Böhi, M. F. Riedel, J. Hoffrogge, J. Reichel, T. W. Hänsch, and P. Treutlein, *Nat. Phys.* **5**, 592 (2009).
- <sup>8</sup>Y.-J. Lin, I. Teper, C. Chin, and V. Vuletić, *Phys. Rev. Lett.* **92**, 050404 (2004).
- <sup>9</sup>K. K. Das and S. Aubin, *Phys. Rev. Lett.* **103**, 123007 (2009).
- <sup>10</sup>C. D’Errico, M. Zaccanti, M. Fattori, G. Roati, M. Inguscio, G. Modugno, and A. Simoni, *New J. Phys.* **9**, 223 (2007).
- <sup>11</sup>M. Lysebo and L. Veseth, *Phys. Rev. A* **81**, 032702 (2010).
- <sup>12</sup>T. Loftus, C. A. Regal, C. Ticknor, J. L. Bohn, and D. S. Jin, *Phys. Rev. Lett.* **88**, 173201 (2002).
- <sup>13</sup>C. A. Regal and D. S. Jin, *Phys. Rev. Lett.* **90**, 230404 (2003).

- <sup>14</sup>Y.-J. Lin, A. R. Perry, R. L. Compton, I. B. Spielman, and J. V. Porto, *Phys. Rev. A* **79**, 063631 (2009).
- <sup>15</sup>S. Händel, A. L. Marchant, T. P. Wiles, S. A. Hopkins, and S. L. Cornish, *Rev. Sci. Instrum.* **83**, 013105 (2012).
- <sup>16</sup>J. M. McGuirk, D. M. Harber, J. M. Obrecht, and E. A. Cornell, *Phys. Rev. A* **69**, 062905 (2004).
- <sup>17</sup>D. M. Harber, J. M. Obrecht, J. M. McGuirk, and E. A. Cornell, *Phys. Rev. A* **72**, 033610 (2005).
- <sup>18</sup>All the parts underwent an Alconox cleaning (in an ultrasonic bath for the smaller parts) followed by a lengthy rinse in water (tap water followed by consumer-grade distilled water). Once the parts are dry and show no watermarks (if they do then they are washed and rinsed again), then they are cleaned with trichloroethylene to remove any heavy oil contamination, followed by multiple rinses with laboratory-grade acetone and then multiple rinses with laboratory-grade methanol. We apply a final rinse with optics-grade methanol to all the parts. All of the vacuum parts are left to dry on a UHV-grade aluminum foil bed (All-Foils) and covered with the same foil. We use standard powder free nitrile gloves while handling the parts during the initial cleaning stages, but switch over to pure latex clean-room quality gloves (KimTech) for the final rinses and attempt to minimize contact between the gloves and the solvents.
- <sup>19</sup>We begin the bake-out with only the turbo pump and keep the ion pumps off, while baking them out at 200 °C. We also turn on the SAES dispensers at 6 A for 6 min and briefly activate the TSP to clean its surfaces. After 11 days of bake-out, we valve off the turbo with the all-metal angle valve and turn-on the ion pumps for the remaining 3 days of the bake-out.
- <sup>20</sup>K. Lindquist, M. Stephens, and C. Wieman, *Phys. Rev. A* **46**, 4082 (1992).
- <sup>21</sup>S. Aubin, E. Gomez, L. A. Orozco, and G. D. Sprouse, *Rev. Sci. Instrum.* **74**, 4342 (2003).
- <sup>22</sup>H. J. Lewandowski, D. M. Harber, D. L. Whitaker, and E. A. Cornell, *J. Low Temp. Phys.* **132**, 309 (2003).
- <sup>23</sup>J. J. Snyder, R. K. Raj, D. Bloch, and M. Ducloy, *Opt. Lett.* **5**, 163 (1980).
- <sup>24</sup>S. Martínez, L. Hernández, D. Reyes, E. Gomez, M. Ivory, C. Davison, and S. Aubin, *Rev. Sci. Instrum.* **82**, 046102 (2011).
- <sup>25</sup>R. A. Nyman, G. Varoquaux, B. Villier, D. Sacchet, F. Moron, Y. Le Coq, A. Aspect, and P. Bouyer, *Rev. Sci. Instrum.* **77**, 033105 (2006).
- <sup>26</sup>S. Aubin, M. H. T. Extavour, S. Myrskog, L. J. LeBlanc, J. Estève, S. Singh, P. Scrutton, D. McKay, R. McKenzie, I. D. Leroux, A. Stummer, and J. H. Thywissen, *J. Low Temp. Phys.* **140**, 377 (2005).
- <sup>27</sup>M. Greiner, I. Bloch, T. W. Hänsch, and T. Esslinger, *Phys. Rev. A* **63**, 031401 (2001).
- <sup>28</sup>B. Battelier, “Gaz bidimensionnel de bosons ultra-froids: Nouvelle expérience de condensation de Bose-Einstein,” Ph.D. thesis (Université Paris VI, 2007).
- <sup>29</sup>While this analog control method is less accurate than a purely digital method, we estimate that the resulting frequency stability is about 1 kHz over the 1–20 MHz range, sufficient for reliable and stable production of BEC.
- <sup>30</sup>R. Grimm, M. Weidemüller, and Y. B. Ovchinnikov, *Adv. At. Mol. Opt. Phys.* **42**, 95 (2000).
- <sup>31</sup>V. Bagnato, D. E. Pritchard, and D. Kleppner, *Phys. Rev. A* **35**, 4354 (1987).
- <sup>32</sup>M. Landini, S. Roy, L. Carcagní, D. Trypogeorgos, M. Fattori, M. Inguscio, and G. Modugno, *Phys. Rev. A* **84**, 043432 (2011).
- <sup>33</sup>S. Aubin, S. Myrskog, M. H. T. Extavour, L. J. LeBlanc, D. McKay, A. Stummer, and J. H. Thywissen, *Nat. Phys.* **2**, 384 (2006).
- <sup>34</sup>V. Bolpasi and W. von Klitzing, *Rev. Sci. Instrum.* **81**, 113108 (2010).
- <sup>35</sup>While this article was under review, we obtained 300 mW of 767 nm trapping light by converting the potassium tapered amplifier to a double-pass configuration.
- <sup>36</sup>T. A. Byrd, M. K. Ivory, A. J. Pyle, S. Aubin, K. A. Mitchell, J. B. Delos, and K. K. Das, *Phys. Rev. A* **86**, 013622 (2012).
- <sup>37</sup>L. De Sarlo, P. Maioli, G. Barontini, J. Catani, F. Minardi, and M. Inguscio, *Phys. Rev. A* **75**, 022715 (2007).